# Izod impact strength of polystyrene-based blends containing low molecular weight polybutadiene

**E. Piorkowska*, A. S. Argon and R. E. Cohen†‡**
*Department of Mechanical Engineering and †Department of Chemical Engineering, Massachusetts Institute of Technology, Cambridge, MA 02139-4307, USA*
*(Received 31 January 1992; revised 14 December 1992)*

Experiments were conducted to determine the influence on impact strength of small amounts of low molecular weight polybutadiene pools dispersed within the glassy matrix of high impact polystyrene (HIPS)/polystyrene blends or acrylonitrile–butadiene–styrene (ABS)/polystyrene blends. The blends of HIPS and polystyrene or ABS and polystyrene were formulated to obtain materials containing small amounts of composite particles to act as craze initiators. Izod impact tests were conducted on standard single notched samples. The fracture surfaces of the Izod specimens and of double-notched tensile specimens were studied by means of scanning electron microscopy, and the internal morphologies of the blends were examined by transmission electron microscopy. Addition of low molecular weight polybutadiene does not increase the impact strength of the blends because, at the high strain rates of the Izod test, the low molecular weight polybutadiene loses its effectiveness as a local plasticizer of craze fibrils. Tensile tests at various strain rates were conducted in order to estimate the strain rate where the mobility of the low molecular weight polybutadiene cannot keep up with the rate of craze propagation through the polystyrene matrix; this critical strain rate is in the region of $10^{-2}\,s^{-1}$ at 20°C for the particular low molecular weight polybutadiene (3400 g $mol^{-1}$, 74% 1,4 microstructure) employed here.

**(Keywords: impact strength; blends; polybutadiene)**

## INTRODUCTION

The well-known high impact polystyrene (HIPS) or acrylonitrile–butadiene–styrene (ABS) type mechanism for toughening glassy polymers by crazing relies on incorporation of rubber particles into a glassy polymer matrix[1–3]. The particles act as craze initiators and thereby promote the dilatational plastic deformation of the normally brittle polymer. In order to be effective in the toughening process, the particles must be very compliant and must adhere to the matrix; the particle effectiveness also depends on particle size, which must exceed a certain critical value which in turn depends on the properties of both particle and surrounding matrix[4,5].

Recent studies[6–8] have revealed a new path to toughened glassy polymers. Low molecular weight liquid polybutadiene (PB) pools dispersed in polystyrene (PS) promote propagation of crazes at relatively low stress levels. When intersected by an advancing craze, the PB pools drain their content onto the craze surfaces and, due to increased solubility of the low molecular weight PB in PS resulting from the negative pressure at the craze tip and at the stems of the craze fibrils[7], rapid sorption of PB into PS surface layers occurs. This locally dissolved PB plasticizes the craze fibrils and thereby reduces the craze flow stress. At the lower craze flow stresses, propagating crazes survive encounters with adventitious flaws, and increased elongation and toughness can be achieved by the sample[6]. The molecular weight and chemical structure of the PB are important parameters since they influence its ability to wet the craze surfaces and to diffuse into the craze fibrils[8]. The PB content is also an important parameter because it influences the number and size of the prepackaged particles of potential diluent. An increase of PB content results in increases in the number and size of PB particles; initially these increases lead to further reduction in craze flow stress and further enhancement of the elongation achieved by the sample. However, if there are any unusually large PB cavities, they initiate premature craze fracture, thus it is necessary to maintain the particle size below about 0.5 $\mu m$[8].

Although the presence of low molecular weight PB pools within the glassy PS matrix promotes the growth of crazes initiated on the surfaces of the sample, there is not a corresponding favourable influence on craze initiation. Therefore the next step[8] was to combine the roles of two toughening mechanisms by preparation of blends containing not only low molecular weight PB but also craze initiating particles; this was achieved by addition of some HIPS or ABS to blends containing pools of low molecular weight PB which resulted in a substantial increase of elongation[8].

The description of this new mechanism of toughening of PS[6–8] was based on results of tensile tests conducted at low strain rates in the region of $10^{-4}\,s^{-1}$. Certain of the processes involved in the toughening mechanism,

* Permanent address: Centre of Molecular and Macromolecular Studies, Polish Academy of Sciences, 90 363 Lodz, Poland
‡ To whom correspondence should be addressed

0032-3861/93/214435-10

such as wetting of craze surfaces by PB and sorption of PB into the craze fibrils, require time to be accomplished, and the effectiveness of this toughening mechanism should therefore depend on the strain rate. In this paper the results of Izod impact tests are reported; these tests were conducted on PS-based blends containing low molecular weight PB and a certain amount of HIPS or ABS. For comparison, PS/HIPS and PS/ABS blends were also studied, as well as pure HIPS and ABS samples. The fracture surfaces were examined by scanning electron microscopy (SEM). The morphology of samples was studied by transmission electron microscopy (TEM). Tensile tests at various strain rates were also conducted, and double-notched specimens were fractured at 50 $\mu$m min$^{-1}$ to investigate the fracture process under conditions of slow drawing.

## EXPERIMENTAL

### *Preparation of blends*

Four different blends were prepared: 87 wt% PS, 3 wt% PB, 10 wt% HIPS (PS/PB/HIPS); 90 wt% PS, 10 wt% HIPS (PS/HIPS); 87 wt% PS, 3 wt% PB, 10 wt% ABS (PS/PB/ABS); and 90 wt% PS, 10 wt% ABS (PS/ABS). Pure ABS and pure HIPS materials were also processed using similar methods. The PS used in this study was Polysar Inc. product number 101-300. HIPS was manufactured by Mobil and the ABS was supplied by Polysciences, Inc. PB having $M_w = 3400$ g mol$^{-1}$ and 74% 1,4 microstructure was purchased from Scientific Polymer Products, Inc.

The compositions described above were chosen because it was known from ref. 8 that the ternary blend materials exhibit very high levels of toughness in low strain rate tensile tests. In order to obtain a good dispersion of small PB pools, we used a method of preparation based on precipitation of dissolved polymers into a non-solvent. Toluene solutions containing 3 wt% of polymer were prepared, stored for several days and then precipitated into methanol; each 300 ml portion of polymer solution was added dropwise into 1500 ml of stirred methanol. In the particular case of pure ABS, 2100 ml of methanol was used. The fine powdery materials collected after precipitation were dried in a vacuum oven for 24 h at room temperature and for the next 24 h at temperatures in the range of 60–70°C. After drying, the polymers were cooled to room temperature while maintaining vacuum.

### *Preparation of samples for Izod impact test*

The bars for the impact test were obtained from polymer powders in two-step compression moulding at 177°C. Because of the sensitivity of PB to oxidation, an effort was made to minimize the time of heating of the blends. Preliminary films 0.5 mm thick were obtained during a 1.5 min moulding of the powder between aluminium plates. After cooling, they were cut into pieces which were placed in a hot aluminium mould between aluminium plates lined with Mylar film. After 2.5–3 min, pressure was applied and held for 2 min at 177°C. Then the press was cooled to room temperature over a period of several minutes. This procedure resulted in bubble-free bars of all the materials. Samples of ABS and HIPS were also obtained from pellets applying the same two-step moulding procedure.

The sizes of samples were chosen to conform to ASTM D256: the length in the range 60.30–63.50 mm, the width $12.70 \pm 0.15$ mm and the thickness 4.1–4.2 mm. The impacted and opposing surfaces of the bars were ground and polished to make them smooth and parallel. The smoothness of lateral surfaces was ensured by using the Mylar film during moulding. The samples were notched according to ASTM D256; the notches had an included angle of $45 \pm 1°$, and a radius of curvature at the apex of $0.25 \pm 0.05$ mm. The depth of the material remaining in the bar behind the notch was $10.16 \pm 0.05$ mm and the length of the impacted end was in the range 31.5–32.0 mm. Before testing, the samples were conditioned in the laboratory atmosphere for at least 48 h.

### *Izod impact test*

The impact test was conducted at room temperature by means of a cantilever beam impact machine delivering a maximum energy of 2.8 J. The velocity of the pendulum at the point where it strikes the sample was 3.4 m s$^{-1}$. Eight or nine samples of each material were tested.

### *Morphology examination*

The fracture surfaces obtained during impact tests were coated with thin layers of gold and examined in a scanning electron microscope. Small pieces of the material adjacent to the fracture surfaces were cut from the impacted bars 1 mm behind the notch and stained in 1 wt% aqueous solution of $OsO_4$, which causes crosslinking and staining of the PB phase. Ultrathin sections (600–800 Å) were then cut at right angles to the fracture planes. The sections were microtomed in such a way that one edge of the section was part of the fracture surface. The sections were examined in a Phillips 300 transmission electron microscope.

### *Tensile testing*

Films of 0.6–0.8 mm thickness were prepared from powders of PS/PB/HIPS, PS/HIPS, PS/PB/ABS and PS/ABS by compression moulding between aluminium plates lined with Mylar film. The compression moulding was conducted at 177°C for 3 min after which the press was cooled to room temperature over a period of several minutes. Oar-shaped specimens with 6.35 mm gauge length and 3.18 mm gauge width were cut from the films. The tensile tests were performed on an Instron tensile testing machine at strain rates of $2.6 \times 10^{-4}$, $1.3 \times 10^{-3}$, $2.6 \times 10^{-3}$ and $2.6 \times 10^{-2}$ s$^{-1}$. Three to five specimens of each blend were tested at each strain rate.

### *Drawing of notched samples*

Films (0.6–0.8 mm thick) were prepared from precipitated powders of PS/PB/HIPS, PS/HIPS, PS/PB/ABS, PS/ABS as well as pure HIPS and ABS as described above. In addition, films from ABS and HIPS pellets were also prepared by compression moulding. Samples with the same geometry and sizes as those used for Izod impact tests (except for the thickness, which was within the range 0.6–0.8 mm) were cut out from the moulded films. They were notched symmetrically on opposite sides in the middle of the sample length. Notches were cut in the samples in exactly the same way as in the Izod specimens. The distance between the tips of the opposing notches was kept constant at $7.62 \pm 0.05$ mm in all samples. Prior to testing, all samples were conditioned in the laboratory atmosphere for several weeks.

The drawing of the double-notched specimens was

performed on an Instron tensile testing machine. Samples were clamped at a distance of 25 mm from the centre of the sample. The drawing was conducted at a rate of 50 $\mu$m min$^{-1}$, and the force was recorded during the entire process until the end of fracture. The fracture surfaces of all blends as well as of pure ABS and HIPS were coated with gold and examined by SEM.

## RESULTS

The Izod impact energies (per unit thickness) of all materials tested are listed in *Table 1*. The impact energies obtained for PS/PB/ABS and PS/ABS are low and are comparable to the impact energies reported for pure PS[1]. Pure ABS materials, as expected, exhibited several times higher impact energies; the samples obtained from precipitated and moulded ABS had somewhat lower impact energy than those obtained from direct moulding of the original pellets. The impact energy of PS/HIPS blend was also low and close to the values obtained for the PS/ABS and PS/PB/ABS materials. PS/PB/HIPS exhibited some enhancement of impact energy, higher by 70% than the value obtained for PS/HIPS material, suggesting some improvement of toughness due to the presence of the low molecular weight PB. The impact energy of pure HIPS materials was several times higher than the impact energy of blends containing HIPS. The value obtained for precipitated HIPS was somewhat lower than that for HIPS from pellets. Visual examination showed intense whitening in the pure ABS and HIPS samples. Slightly whitened zones of width 0.7–0.8 mm near the notches were seen on the fracture surfaces of the PS/PB/HIPS samples.

SEM micrographs of fracture surfaces are shown in *Figures 1–6*. The crack propagated from left to right in all cases. At low magnification the fracture surfaces of pure HIPS appear flat, without any ridges or other pronounced features. At higher magnification (*Figure 1*) one can see that the fracture surface is highly developed and shows evidence of plastic deformation. The rubber particles are also seen. The fracture surface character is essentially the same from the notch to the end of fracture. No difference was noticed between the precipitated HIPS and that obtained from pellets.

Micrographs obtained approximately 1 mm from the notch fronts are shown in *Figures 2a,b* and *3a,b* for PS/HIPS and PS/PB/HIPS, respectively. *Figure 2a* shows bands of brittle fracture in PS/HIPS blends resulting from the repeated arrest and re-initiation of the fracture.

**Table 1** Izod impact strength of tested materials

| Material | Izod impact strength (J cm$^{-1}$) | |
|---|---|---|
| | Average | Standard deviation |
| PS/HIPS | 0.125 | 0.0136 |
| PS/PB/HIPS | 0.216 | 0.0233 |
| HIPS[a] | 0.788 | 0.0244 |
| HIPS[b] | 0.987 | 0.0438 |
| PS/ABS | 0.119 | 0.0106 |
| PS/PB/ABS | 0.130 | 0.0037 |
| ABS[a] | 0.501 | 0.0097 |
| ABS[b] | 0.769 | 0.0166 |

[a] Obtained from precipitated material
[b] Obtained from pellets

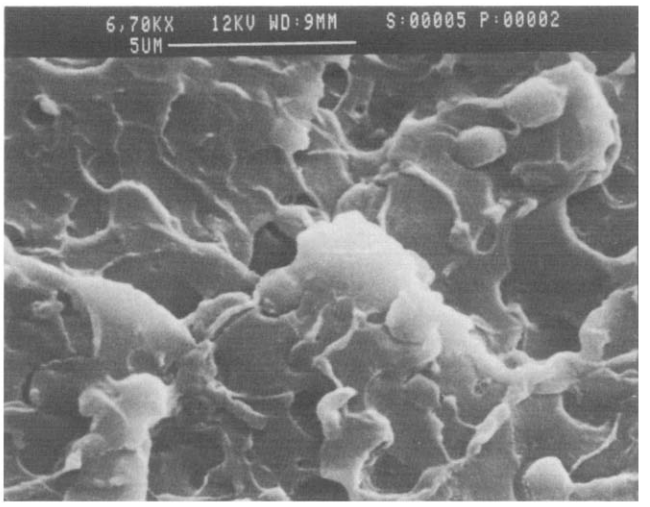


**Figure 1** SEM micrograph of fracture surface of HIPS bar obtained from precipitated material

Higher magnification reveals the 'mackerel' pattern which results from the biplanar fracture of crazes[9,10]. The fracture surface of PS/PB/HIPS blends (*Figure 3a*) also exhibits bands of brittle fracture; however, they are more highly developed surfaces compared to the PS/HIPS blend. There are no flat zones near the ends of the bands. Higher magnification reveals a 'mackerel' structure (*Figure 3b*) similar to that seen in *Figure 2b*. Additionally, numerous holes of submicrometre size are seen, which indicates that fracture propagated through the PB pools. *Figures 2c* and *3c* show patterns of bands of brittle fracture near the notches in PS/HIPS and PS/PB/HIPS blends at low magnification. In the case of the PS/HIPS blend the bands emanate from the notch, but in the PS/PB/HIPS blend the bands appear behind a considerable flat zone about 0.8 mm wide adjacent to the notch. In both blends the morphology of the area near the notch seen at high magnification is very similar to that shown in *Figures 2b* and *3b*. However, in the case of PS/PB/HIPS, a small amount of plastically deformed material, in the form of pieces protruding from the surface, appears in the area next to the notch (*Figure 3c*).

The fracture surfaces of ABS bars obtained from pellets and precipitated material look similar over the whole fracture surface. As in the case of HIPS, the surfaces of ABS samples seen at low magnification are flat. Higher magnification (*Figure 4*) reveals highly developed fracture surfaces and a certain amount of plastically deformed material. The fracture surface of ABS specimens obtained from pellets is somewhat more developed than for specimens obtained from precipitated material. The fracture surface of PS/ABS and PS/PB/ABS blends seen at low magnification are very similar to the pictures shown in *Figures 2a* and *2c* for the PS/HIPS blend. Bands of brittle fracture emanating from the notches are visible in both cases. Details of fracture morphology are shown in *Figures 5* and *6* for PS/ABS and PS/PB/ABS blends, respectively. Numerous ABS particles and holes left by particles are seen in *Figures 5* and *6*. Particles are located in cavities, which suggests widespread decohesion of particles during fracture. No significant differences were noticed between fracture surfaces of PS/PB/ABS and PS/ABS blends. The areas near the notches seen at higher magnifications look similar to *Figures 5* and *6*.

TEM examination of ultrathin sections of PS/HIPS and PS/ABS blends (*Figures 7* and *8*, respectively) show

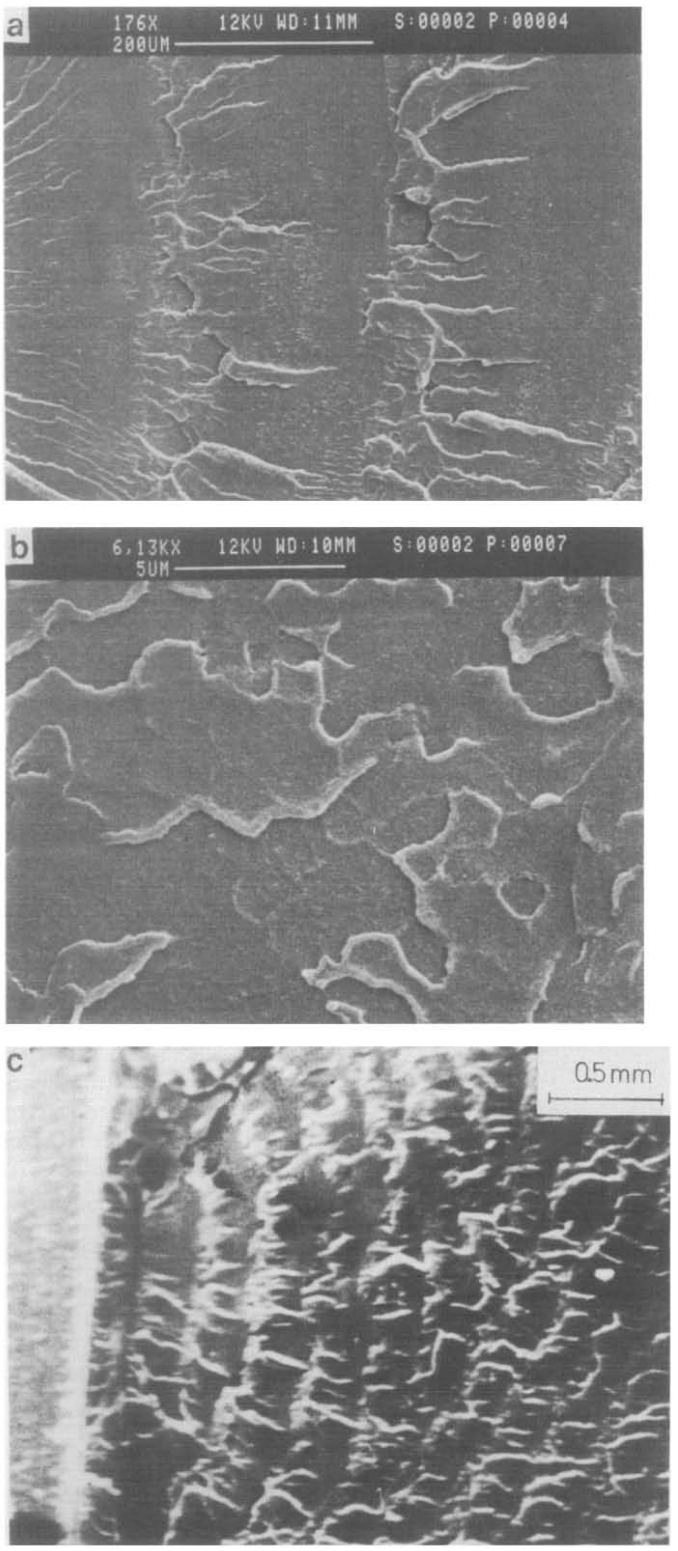


**Figure 2** SEM micrograph of fracture surface 1 mm ahead of the notch tip of PS/HIPS blend: (a) overview; (b) detail; (c) low magnification view of area near the notch

the rubber particles embedded in the PS matrix. The morphology of associated blends with PB is shown in *Figures 9* and *10*. Besides the typical ABS or HIPS inclusions, submicrometre pools of PB are dispersed within the PS matrix. The examination of pure ABS and HIPS materials revealed typical particle structures, which were identical in samples obtained from pellets and from precipitated materials. Examination of sections adjacent to fracture surfaces of ABS and HIPS bars showed numerous crazes originating from the composite particles. The area close to the fracture surface of a pure HIPS sample is shown in *Figure 11*.

The results of Instron tensile tests are depicted in *Figures 12–15*. Typical stress–strain curves are plotted in these figures, while average craze flow stresses and average elongations, obtained by testing three to five

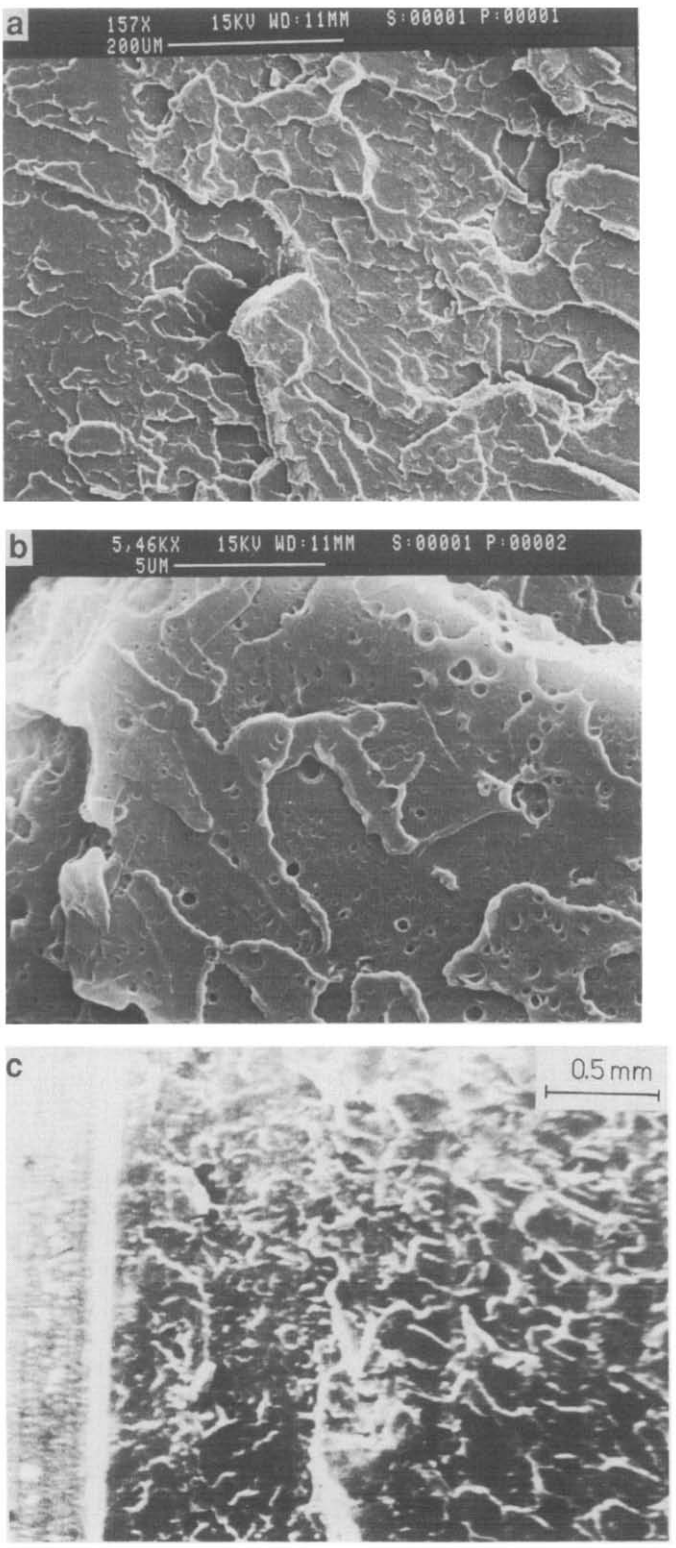


**Figure 3** SEM micrograph of fracture surface 1 mm behind the notch of PS/PB/HIPS blend: (a) overview; (b) detail; (c) low magnification view of area near the notch

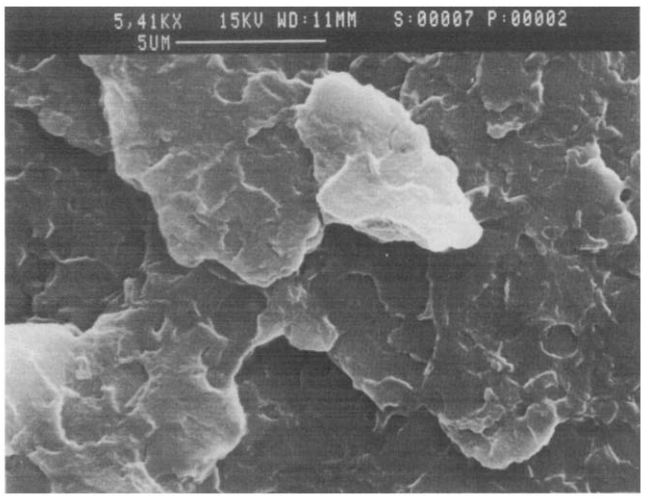


**Figure 4** SEM micrograph of fracture surface of ABS bar obtained from precipitated material

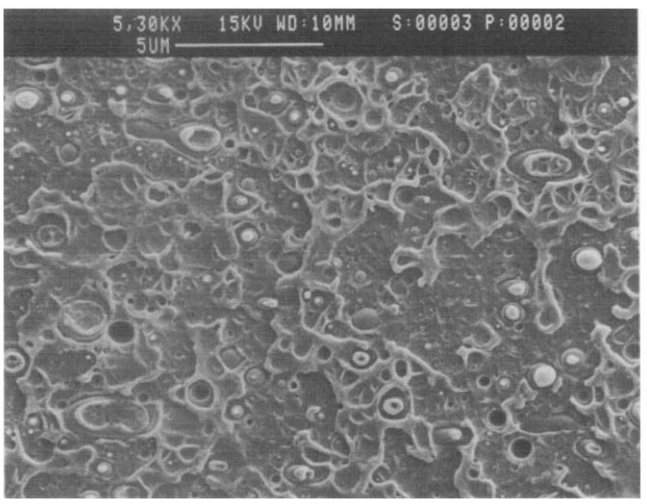


**Figure 5** SEM micrograph of fracture surface 1 mm behind the notch of PS/ABS blend: detail


**Figure 6** SEM micrograph of fracture surface 1 mm behind the notch of PS/PB/ABS blend: detail

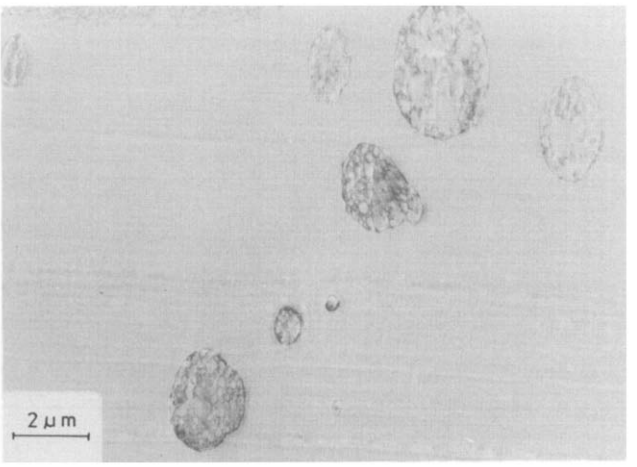


**Figure 7** TEM micrograph of PS/HIPS

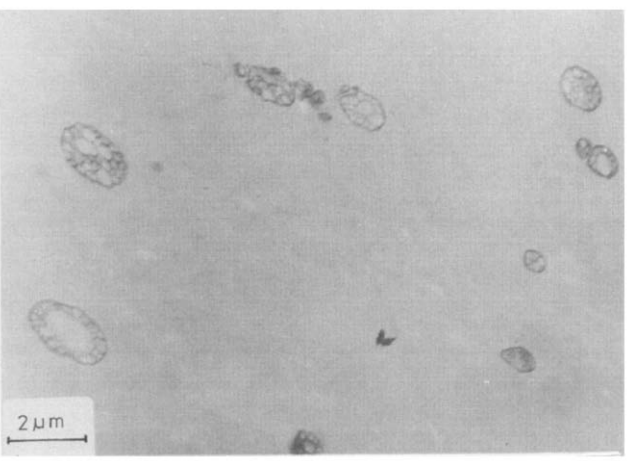


**Figure 8** TEM micrograph of PS/ABS

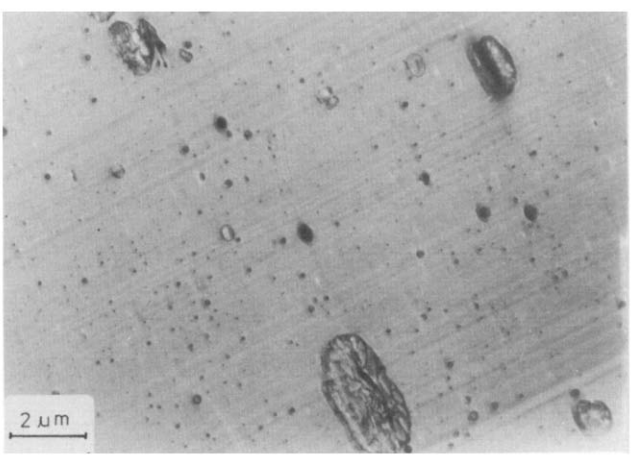


**Figure 9** TEM micrograph of PS/PB/HIPS

blend specimens, are listed in *Table 2* for various strain rates. The PS/HIPS samples behave similarly at all strain rates. The craze flow stress increases slightly from 35.7 MPa at a strain rate of $2.6 \times 10^{-4}$ s$^{-1}$ to 38.9 MPa at $2.6 \times 10^{-2}$ s$^{-1}$, while total elongations do not change and are close to 0.08 (plastic elongations of only 0.03). On the other hand, the results of tensile tests of PS/PB/HIPS samples depend strongly on the strain rate. The craze flow stress increases from 17.0 to 35.3 MPa with

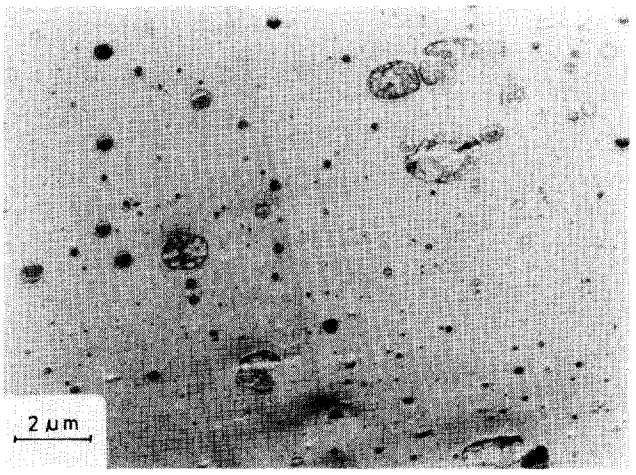


**Figure 10** TEM micrograph of PS/PB/ABS

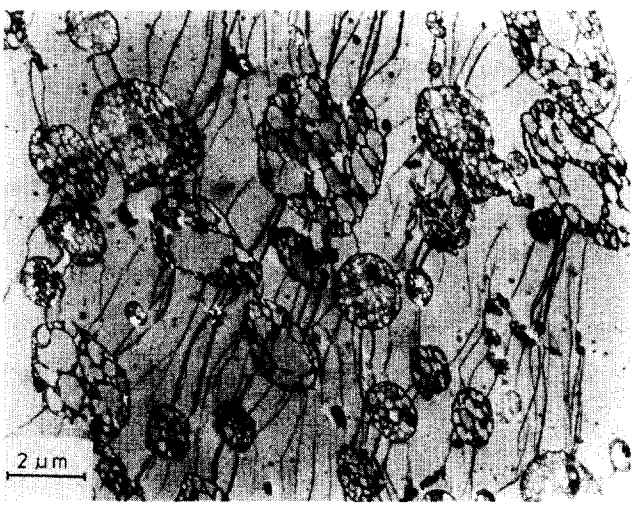


**Figure 11** TEM micrograph of ultrathin section of the region adjacent to the fracture surface of HIPS

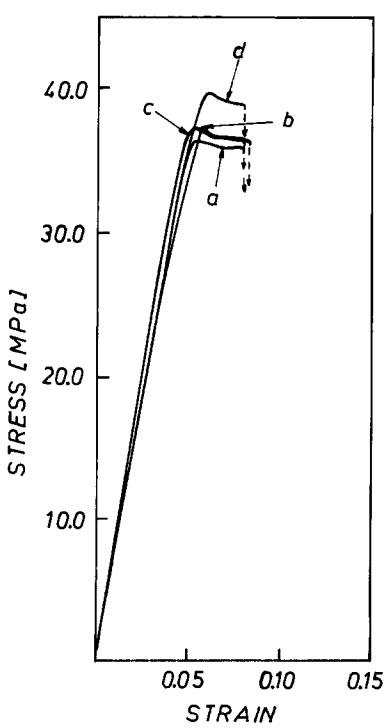


**Figure 12** Stress–strain curves of PS/HIPS blend obtained at various strain rates: a, $2.6 \times 10^{-4}\,s^{-1}$; b, $1.3 \times 10^{-3}\,s^{-1}$; c, $2.6 \times 10^{-3}\,s^{-1}$; d, $2.6 \times 10^{-2}\,s^{-1}$

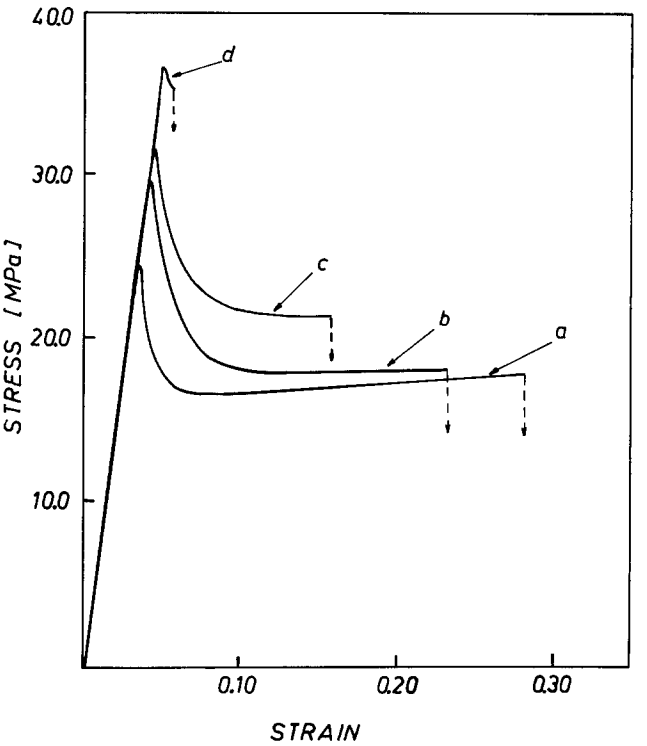


**Figure 13** Stress–strain curves of PS/PB/HIPS blend obtained at various strain rates: a, $2.6 \times 10^{-4}\,s^{-1}$; b, $1.3 \times 10^{-3}\,s^{-1}$; c, $2.6 \times 10^{-3}\,s^{-1}$; d, $2.6 \times 10^{-2}\,s^{-1}$

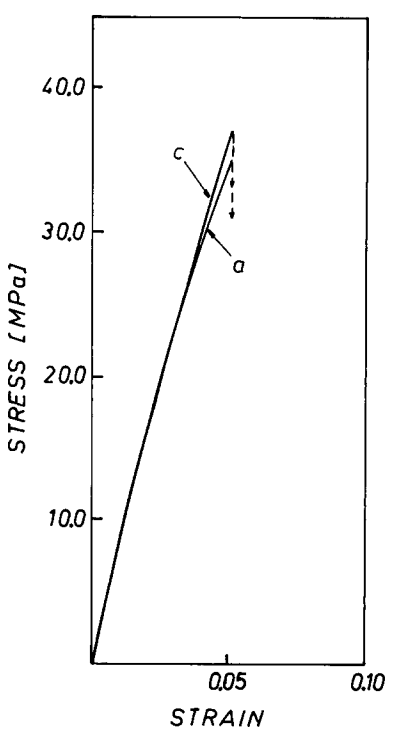


**Figure 14** Stress–strain curves of PS/ABS blend obtained at various strain rates: a, $2.6 \times 10^{-4}\,s^{-1}$; c, $2.6 \times 10^{-3}\,s^{-1}$

increasing strain rate, while total elongation decreases from 0.28 to 0.06. The clear difference between PS/HIPS and PS/PB/HIPS at low strain rates completely disappears at the highest tensile strain rate employed. Very prominent yield drops are apparent in the curves, indicating the difficulty in initiating craze plasticity and the comparative ease of perpetuating it.

The PS/ABS and PS/PB/ABS blends behaved much

like their HIPS counterparts. The PS/ABS samples do not show any plastic deformation; they break at high stress levels of 35.4 and 37.8 MPa at strain rates of $2.6 \times 10^{-4}$ and $2.6 \times 10^{-3}\ s^{-1}$, respectively, with behaviour identical to that of pure PS. The average total elongation of samples was 0.05 in both cases (with essentially no plastic elongation). The craze flow stress and elongation of PS/PB/ABS samples depend strongly on the strain rate: flow stress changes from 19.1 to 23.1 MPa, and total elongation varies from 0.35 to 0.16 with increase of the strain rate from $2.6 \times 10^{-4}$ to $2.6 \times 10^{-3}\ s^{-1}$, as shown in *Figure 15*. At a strain rate of $2.6 \times 10^{-2}\ s^{-1}$ the PS/PB/ABS blend no longer shows any plastic deformation; it breaks at a stress level of 38.8 MPa and a total elongation of 0.05, essentially identical to the values exhibited by the PS/ABS material.

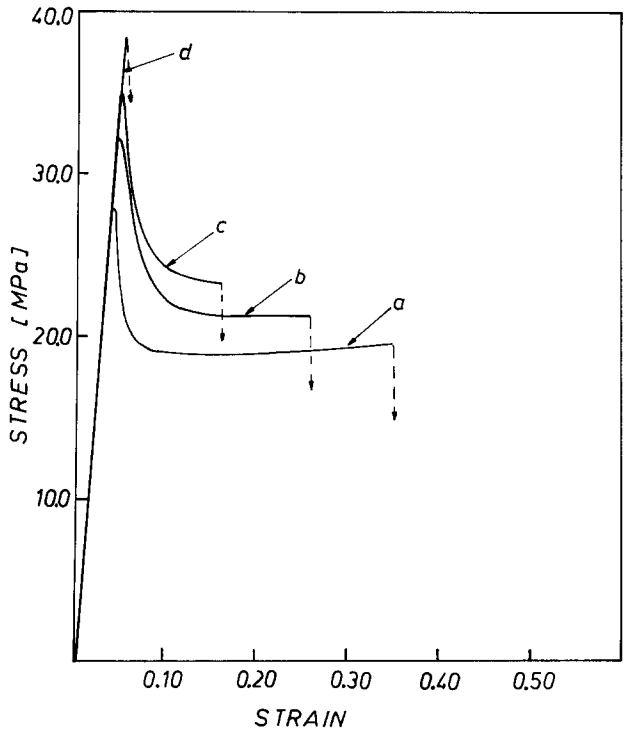


**Figure 15** Stress–strain curves of PS/PB/ABS blend obtained at various strain rates: a, $2.6 \times 10^{-4}\ s^{-1}$; b, $1.3 \times 10^{-3}\ s^{-1}$; c, $2.6 \times 10^{-3}\ s^{-1}$; d, $2.6 \times 10^{-2}\ s^{-1}$

**Table 2** The average craze flow stress (A, MPa) and average elongation (B) achieved by samples tested at various strain rates

| | Strain rate ($s^{-1}$) | | | | | | | |
|---|---|---|---|---|---|---|---|---|
| | $2.6 \times 10^{-4}$ | | $1.3 \times 10^{-3}$ | | $2.6 \times 10^{-3}$ | | $2.6 \times 10^{-2}$ | |
| | A | B | A | B | A | B | A | B |
| PS/HIPS | 35.7 | 0.08 | 36.6 | 0.08 | 36.5 | 0.08 | 38.9 | 0.08 |
| PS/PB/HIPS | 17.0 | 0.28 | 17.8 | 0.23 | 21.8 | 0.16 | 35.3 | 0.06 |
| PS/ABS | 35.4[a] | 0.05 | – | | 37.8[a] | 0.05 | – | – |
| PS/PB/ABS | 19.1 | 0.35 | 21.1 | 0.26 | 23.1 | 0.16 | 38.8[a] | 0.05 |

[a] No plastic deformation observed

The results of drawing of notched samples are shown in *Figures 16* and *17*. Upon yielding across the ligament, the notches interact in a complex way in establishing the region of plastic deformation and its extent away from the plane of the ligament, making it difficult to determine the dimensions of this zone and the strain distribution in it. However, the distance between the tips of the notches is the same in all samples. Therefore, only the net section stress is presented as a function of crosshead displacement in *Figures 16* and *17*.

The ABS and HIPS materials behave in a similar way. Initially, the net section stress increases linearly with displacement. When whitening due to crazing first appears at the tips of the notches, a downward curvature appears in the force displacement plot. When the whitening spreads over the whole area between the tips of the notches, the net section stress levels off and remains constant until cracks begin propagating from the tips of the notches and cause a decrease in the measured force. The terminal shapes of the curves are associated with increases in crack speed with increasing distance from the notch. When the cracks meet, fracture of the sample is complete.

The PS/ABS blend (*Figure 17*, curve c) fractures rapidly before any whitening is observed. In the PS/HIPS blend (curve a) some plastic deformation due to crazing is observed prior to fracture. PS/PB/HIPS and PS/PB/ABS blends (curves b and d) behave substantially differently from the blends not containing any low molecular weight PB. The observed force–displacement curves are similar to those observed in pure ABS and HIPS. Substantial plastic deformation due to crazing is observed and crack propagation from the tips of notches is accompanied by a gradual reduction of force prior to fracture.

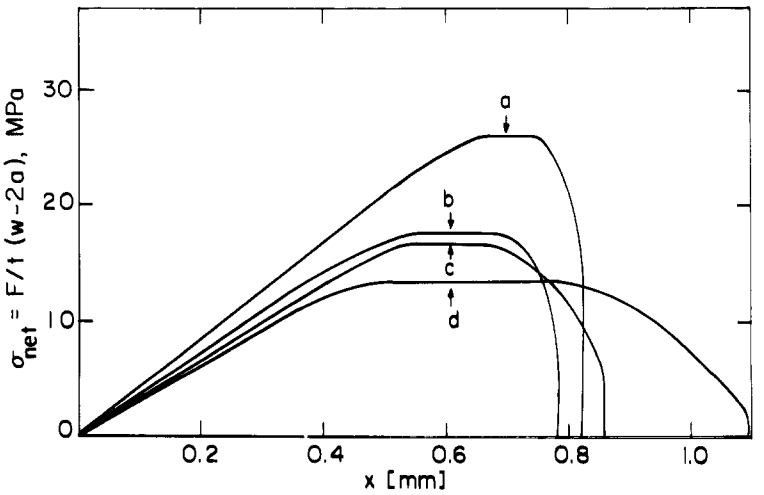


**Figure 16** Net section stress *versus* crosshead displacement recorded during slow drawing of double-notched specimens: a, ABS precipitated; b, ABS from pellets; c, HIPS precipitated; d, HIPS from pellets. The symbols $t$, $w$ and $a$ represent specimen thickness, width and notch depth, respectively

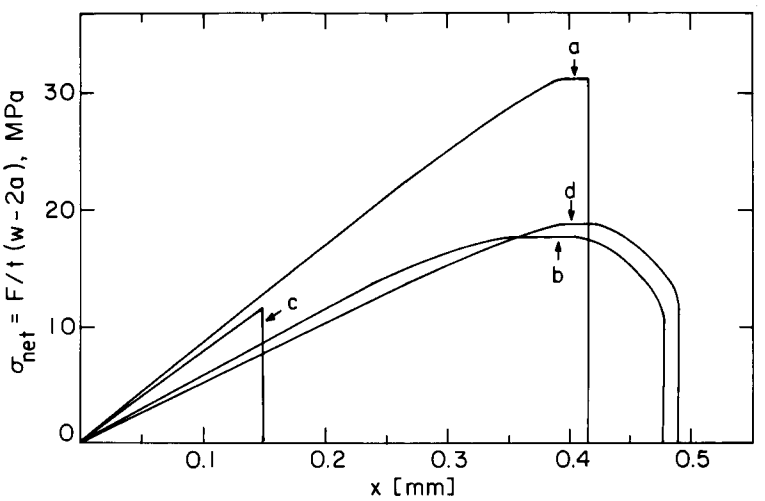


**Figure 17** Net section stress *versus* crosshead displacement recorded during slow drawing of double-notched specimens: a, PS/HIPS; b, PS/PB/HIPS; c, PS/ABS; d, PS/PB/ABS. The symbols *t*, *w* and *a* represent specimen thickness, width and notch depth, respectively

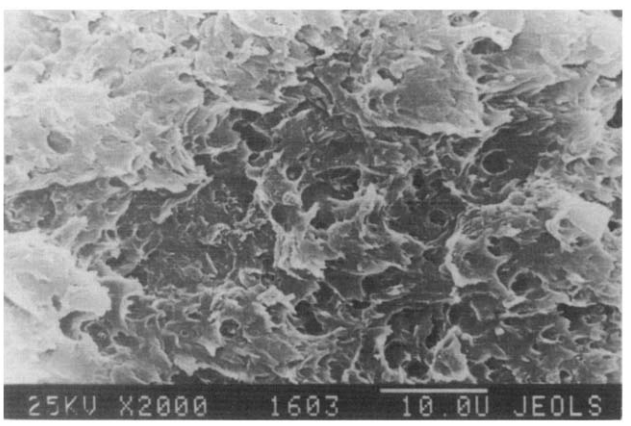


**Figure 18** SEM micrograph of fracture surface of slowly drawn double-notched specimen obtained from precipitated HIPS

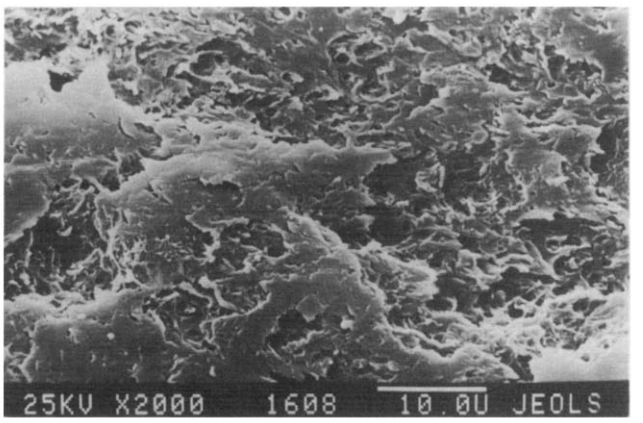


**Figure 19** SEM micrograph of fracture surface of slowly drawn double-notched specimen obtained from precipitated ABS

Examination of fractured double-notched samples by means of light microscopy revealed that all samples, except for the PS/ABS blend, contained whitened crazed zones of elliptical shape located between the tips of opposite notches. The lowest amount of crazed material is seen in the PS/HIPS blend while in PS/PB/HIPS and PS/PB/ABS blends intense whitening is observed, identical to that seen in pure HIPS and ABS. SEM micrographs of fracture surfaces are shown in *Figures 18–23*. The direction of crack propagation was from left to right in all cases except for *Figure 22* (PS/HIPS blend) where the crack propagated from right to left. SEM examination at low magnification reveals flat fracture surfaces of pure HIPS and ABS. Fracture surfaces of HIPS and ABS samples seen at higher magnifications are shown in *Figures 18* and *19*, respectively. The surface is highly developed and a large amount of plastically deformed material is seen in both cases. In the case of ABS, smoother patches are also seen (*Figure 19*), which may result from the rubbing together of the two surfaces after fracture. The fracture surfaces are extensively terraced and have a 'flaky' appearance, indicating multiple fracturing at several levels.

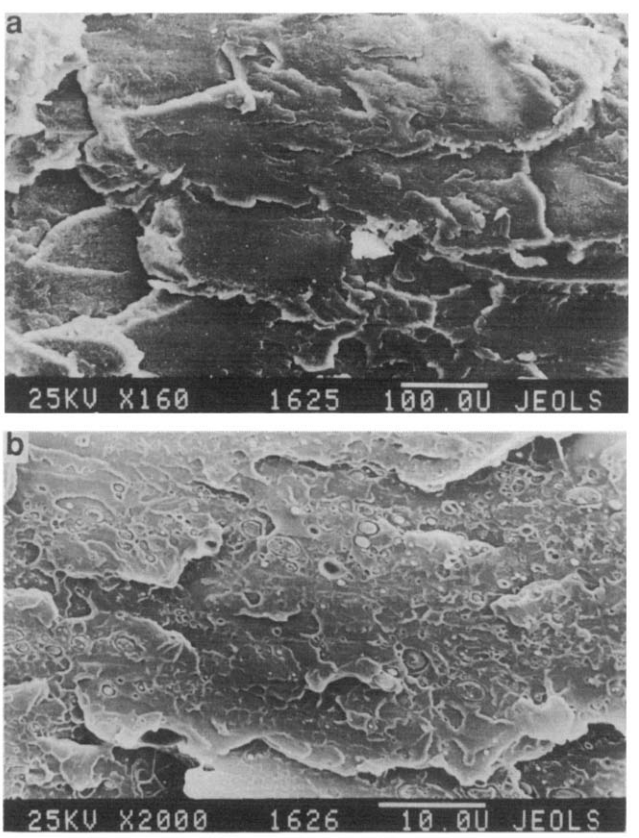


**Figure 20** SEM micrograph of fracture surface of slowly drawn double-notched specimen of PS/ABS blend 1 mm behind the notch: (a) overview; (b) detail

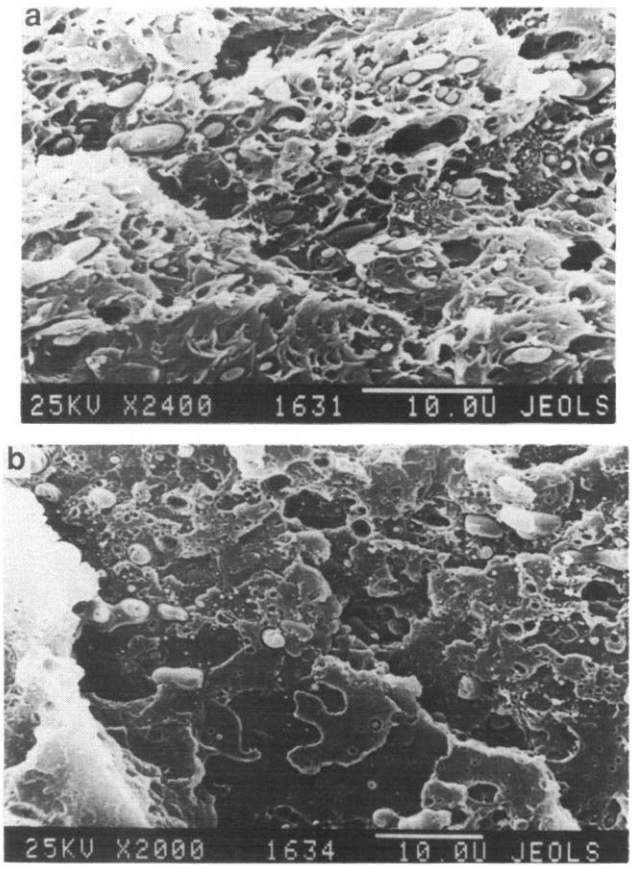


**Figure 21** SEM micrograph of fracture surface of slowly drawn double-notched specimen of PS/PB/ABS blend: (a) 1 mm behind the notch; (b) 2 mm behind the notch

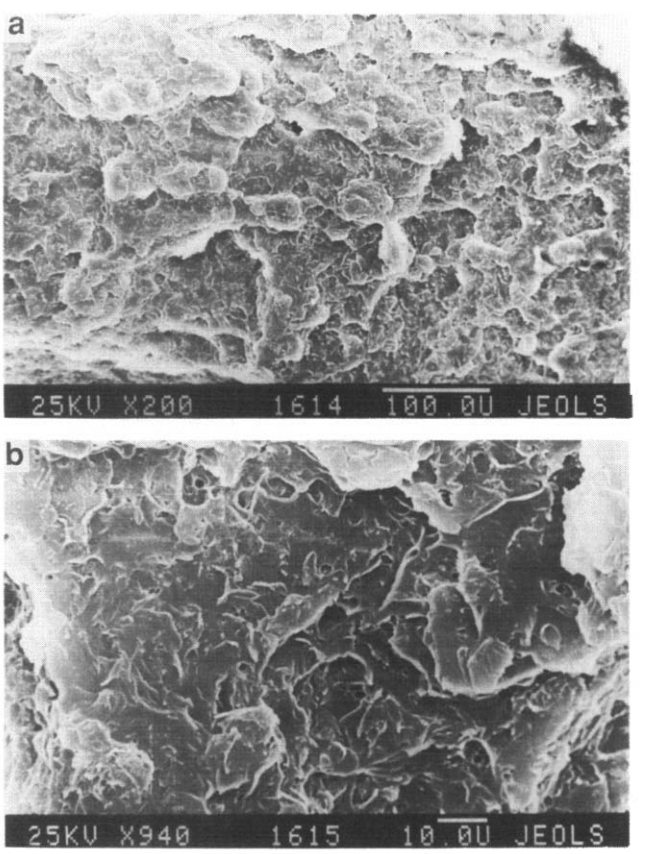


**Figure 22** SEM micrograph of fracture surface in the area next to the notch of slowly drawn double-notched specimen of PS/HIPS blend: (a) overview; (b) detail

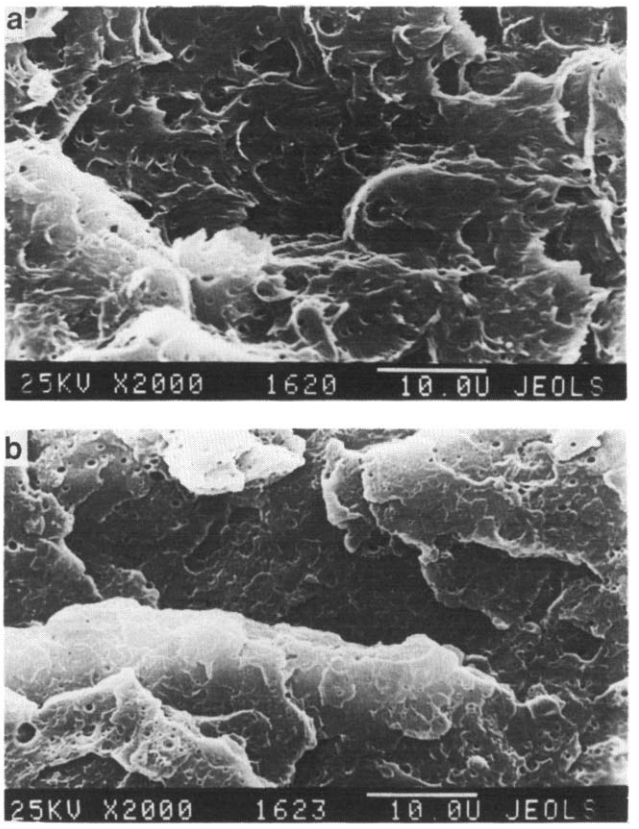


**Figure 23** SEM micrograph of fracture surface of slowly drawn double-notched PS/PB/HIPS specimen: (a) 1 mm behind the notch; (b) 2 mm behind the notch

The fracture surface of the PS/ABS blend shows bands of brittle fracture (*Figure 20a*) emanating from the notch. Higher magnification (*Figure 20b*) reveals the 'mackerel' pattern and the ABS particles and holes left by separation of the particles. Evidence of decohesion of particles from the matrix is visible. The fracture surfaces of PS/PB/ABS blends near the notch examined at low magnification appear flat. At higher magnification, the highly developed fracture surface shows large amounts of plastically deformed material (*Figure 21a*). The ABS particles separated from the matrix are also visible, as well as numerous holes left by particles. The submicrometre size of some of them suggests that they are holes remaining after disruption of the low molecular weight PB pools. Further from the notch, the fracture surfaces change. At low magnification the surface becomes rougher and a few sharp ridges become visible. The surface observed at higher magnification (*Figure 21b*) is less developed, and much less plastically deformed material is visible. Extensive decohesion of particles is apparent. Judging from the white contrast of many particles (poor grounding of particles to substrate) these are almost completely debonded, while some of them are still attached and have a grey appearance.

The fracture surface of the double-notched PS/HIPS blend is shown in *Figures 22a,b*. Near the notch (*Figure 22a*) the surface is rough but without the sharp ridges that are visible farther from the notch. At higher magnification the surface near the notch (*Figure 22b*) is more developed than the area farther from the notch seen at the same magnification. In both cases, a certain amount of plastically deformed material protruding from the surface is visible. The fracture surface of PS/PB/HIPS

near the notch examined at low magnification appears flat. At high magnification, a highly developed flaky surface with large amount of plastically deformed material is seen (*Figure 23a*). Farther from the notch the surface seen at low magnification becomes rougher and a few sharp ridges become visible, similar to the case of PS/PB/ABS. At high magnification (*Figure 23b*) much less plastically deformed material is visible. On the entire surface numerous holes of submicrometre sizes are seen, where apparently the fracture plane has intersected regions of PB pools previously tapped into by crazes. The HIPS particles are not visible in the micrographs of *Figures 22* or *23*, and no debonding of these is visible.

## DISCUSSION

The results of the Izod impact tests show rather decisively that the presence of liquid PB pools within the PS matrix does not increase significantly the high rate impact energy of the material. The results obtained for PS/HIPS and PS/ABS blends are close to the value of impact energy of pure PS, because the content of rubber particles was too small to improve the properties of the materials[11]. The presence of PB in the PS/PB/ABS blend did not significantly influence the fracture behaviour of the material during the impact test. Evidently one of the rate-limiting processes (wetting/spreading of the PB onto the craze surfaces or sorption of the PB into the craze fibrils) was unable to keep up with the advancing fracture plane in the impact experiment. Fracture surfaces showed that the dominant mechanism was separation of ABS particles from the PS matrix in both of the blends containing ABS. In the case of the PS/PB/HIPS blend, the presence of PB particles moderately increased the impact strength (by about 70%) and there was some influence of the PB on the appearance of the fracture surface (*Figure 3b*). The presence of a flat zone of crack initiation behind the notch is usually correlated with an increase in impact energy[12]. It indicates that during relatively slow build-up of stress at the base of the notch, the low molecular weight PB was able to influence the fracture process in this limited region of the specimen.

The results of tensile tests show that at a strain rate near $2.6 \times 10^{-2}\,s^{-1}$ the low molecular weight PB loses its ability to influence the propagation of crazes within the PS matrix. Since strain rates during impact test are of the order $10^{2}\,s^{-1}$, these tensile test results clarify the reasons for the observed inability of the low molecular weight PB to influence significantly the fracture behaviour in Izod tests.

The influence of the low molecular weight PB on fracture of double-notched samples is, however, clearly observed during slow drawing. Because of the difficulties in determining the size and distribution of stress and strain in the net section ligament, it was impossible to determine the strain rate directly. However, for blends containing HIPS one can evaluate a ratio of craze flow stresses, because in slow drawing both blends exhibit substantial plastic deformation. The ratio of craze flow stress of the PS/HIPS blend to that of PS/PB/HIPS is 1.65. The constant elongation rate data listed in *Table 2* show that the flow stress ratio is equal to 1.67 at a deformation rate of $2.6 \times 10^{-3}\,s^{-1}$; at that rate the low molecular weight PB had a significant and favourable influence on toughness. SEM examination of the fracture surfaces of double-notched specimens of blends containing low molecular weight PB reveal that, in the area close to the notch, large amounts of plastic deformation occurred. Evidence of plastic deformation became less pronounced as the distance from the notches (and the crack speed) increased.

Thus, in summary, the enhancement of the toughness imparted by the addition of low molecular weight PB, observed so clearly in low deformation rate tests, becomes inoperative at high deformation rates. For the particular PB employed here, the cutoff rate is in the region of $10^{-2}\,s^{-1}$; impact tests operate at rates as much as four orders of magnitude higher. Examination of the fracture events in our various experiments indicates that the failure of the toughening mechanism does not arise from problems in the size or spatial distribution of the PB particles, but rather from the inability of the PB to drain out of the particles and distribute itself homogeneously within the structure of the advancing crazes. Thus, although properly dispersed droplets of low molecular weight PB can serve as a low-rate toughness enhancer, a much more mobile fluid will be required to make any significant improvement in impact toughness. These conclusions are fully consistent with the comprehensive study of Qin *et al.*[8] which has explored additional dimensions of this novel toughening effect; however, the results indicate that the effect is controlled by diluent mobility and becomes inoperable well below impact strain rates.

## ACKNOWLEDGEMENTS

This work was supported by the NSF/MRL programme under Grant DMR-87-19217 through the MIT Center for Materials Science and Engineering. Partial support of the Center of Molecular and Macromolecular Studies, Polish Academy of Sciences, is also acknowledged.

## REFERENCES

1 Bucknall, C. B. 'Toughened Plastics', Applied Science Publishers, London, 1977
2 Kramer, E. J. in 'Advances in Polymer Science: Crazing' (Ed. H. H. Kaush), Springer, Berlin, 1983, Vol. 52/53
3 Bragaw, C. G. *Adv. Chem. Ser.* 1971, **99**, 86
4 Piorkowska, E., Argon, A. S. and Cohen, R. E. *Macromolecules* 1990, **23**, 3838
5 Dagli, G., Argon, A. S. and Cohen, R. E. in press
6 Gebizlioglu, O. S., Beckham, H. W., Argon, A. S., Cohen, R. E. and Brown, H. R. *Macromolecules* 1990, **23**, 3968
7 Argon, A. S., Cohen, R. E., Gebizlioglu, O. S., Brown, H. R. and Kramer, E. J. *Macromolecules* 1990, **23**, 3975
8 Qin, J., Argon, A. S. and Cohen, R. E. in press
9 Doyle, M. J. *J. Mater. Sci.* 1982, **17**, 204
10 Shah, N. *J. Mater. Sci.* 1988, **23**, 3623
11 Bucknall, C. B., Cote, F. F. P. and Partridge, I. K. *J. Mater. Sci.* 1986, **21**, 301
12 Ward, I. M. 'Mechanical Properties of Solid Polymers', John Wiley, Chichester, 1983, Ch. 12